NANO LETTERS

pubs.acs.org/NanoLett Letter

Monolayer Semiconductor Auger Detector

Colin Ming Earn Chow, Hongyi Yu, John R. Schaibley, Pasqual Rivera, Joseph Finney, Jiaqiang Yan, David Mandrus, Takashi Taniguchi, Kenji Watanabe, Wang Yao, David Henry Cobden,* and Xiaodong Xu*

Cite This: *Nano Lett.* 2020, 20, 5538−5543 Read Online

ACCESS | Metrics & More | Article Recommendations | Supporting Information

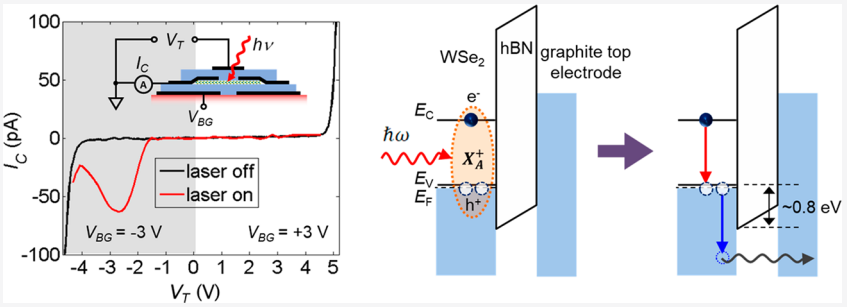

ABSTRACT: Auger recombination in semiconductors is a many-body phenomenon in which the recombination of electrons and holes is accompanied by excitation of other charge carriers. The excess energy of the excited carriers is normally rapidly converted to heat, making Auger processes difficult to probe directly. Here, we employ a technique in which the Auger-excited carriers are detected by their ability to tunnel out of the semiconductor through a thin barrier, generating a current. We use vertical van der Waals heterostructures with monolayer WSe_2 as the semiconductor, with hexagonal boron nitride as the tunnel barrier, and a graphite collector electrode. The Auger processes combined with resonant absorption produce characteristic negative photoconductance. We detect holes Auger-excited by both neutral and charged excitons and find that the Auger scattering is surprisingly strong under weak excitation. Our work expands the range of techniques available for probing relaxation processes in 2D materials.

KEYWORDS: *van der Waals heterostructure, exciton-hole Auger scattering, tunneling barrier, Auger photocurrent, weak excitation*

INTRODUCTION

The two-dimensional (2D) monolayer semiconductors of formula MX_2 (M = Mo, W; X = S, Se) have direct optical band gaps.[1,2] Nevertheless, when pristine exfoliated monolayers are photoexcited, nonradiative recombination usually dominates.[3,4] This is in part a consequence of Auger processes,[5] whose rates are enhanced relative to those in 3D semiconductors because of stronger Coulomb interactions.[6] Among these processes is exciton−exciton annihilation, which dominates at high excitation density,[7−9] and results in either an excited electron in the conduction band or a hole in the valence band. At lower densities, however, opinions vary on the significance of different Auger contributions. One possibility is thermal activation of trapped photocarriers and subsequent increase in the number of delocalized carriers conducive to Auger scattering.[10] This process has been argued to become more important at elevated temperatures,[11,12] although the lack of temperature dependence in some measurements argues against the significance of such processes.[13,14] In addition, in the tungsten-based materials, there are dark exciton ground states which may provide a phonon-assisted Auger channel at low excitation powers,[15] though the significance of this too is unclear.[16] The ambiguous situation is a consequence of the fact that, despite their ubiquity, Auger processes are hard to probe because they are both ultrafast and nonradiative.

In this work, we employ an unconventional photocurrent technique to reveal exciton/trion-hole Auger scattering in monolayer WSe_2. From the dependence of the photocurrent on electrode voltage and excitation energy, we can extract spectral information and band offsets. Figure 1a is a schematic and Figure 1b an optical micrograph of the device which we will focus on in the main text. We obtained consistent results with other similar devices (Supporting Information §6). A WSe_2 monolayer flake is sandwiched between thin hexagonal boron nitride (hBN) dielectric layers, in this case with thicknesses of 8 nm (top) and 10 nm (bottom). Few-layer

Received: May 24, 2020
Revised: June 6, 2020
Published: June 9, 2020

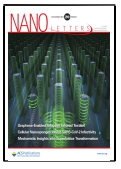

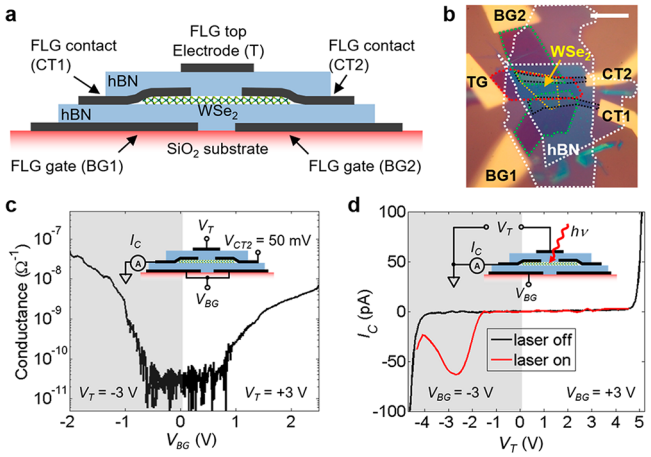

Figure 1. Device geometry and basic characterization. (a) Schematic of a device with monolayer WSe_2 as the active layer. Metal electrodes connecting the few-layer graphene (FLG) flakes are omitted for clarity. (b) Optical micrograph of device 1, measurements on which are presented in the main text. Dotted lines indicate the boundaries of individual flakes, whose thicknesses can be found in Supporting Information §1. Scale bar: 15 μm. (c) Semilog plot of the conductance between CT2 and CT1, as a function of the bottom gate bias V_{BG}, measured at a temperature of 5 K. In the shaded (nonshaded) region, V_T = −3 (+3) V. Inset: measurement configuration. (d) Gate current (I_C) between CT1 and top electrode (T) versus V_T with (red) and without (black) laser illumination at $\hbar\omega$ = 1.71 eV (1 μW at 725 nm). Here CT2 and BG2 are disconnected, as indicated in the inset. In the shaded (nonshaded) region, V_{BG} = −3 (+3) V.

graphene (FLG) is used for electrical contacts CT1 and CT2 to the WSe_2 monolayer. Their separation of about 5 μm defines the WSe_2 channel length. Another FLG piece on top serves both as a gate for electrostatically doping the WSe_2 and as an optically transparent electrode for collecting carriers that cross the hBN barrier. A further pair of split FLG bottom gates, labeled BG1 and BG2, is included for doping the WSe_2 at the respective contacts to reduce the contact resistance. (See the Methods and Supporting Information §1 for fabrication details.)

RESULTS

Device Operating Condition in Auger Photocurrent Mode. Figure 1c shows the conductance between CT1 and CT2 as a function of back-gate voltage V_{BG}, applied equally to BG1 and BG2, measured in the dark with a bias of 50 mV on CT2. We obtain ambipolar operation at low temperature (here 5 K), implying suitably conducting contacts for either electrons or holes, by setting the top electrode voltage V_T to −3 V when $V_{BG} < 0$ and to +3 V when VBG > 0. This dopes the channel with the same carrier type as the contact regions (see Supporting Information §2). In a similar manner, whenever we vary V_T, we set V_{BG} to either +3 or −3 V as appropriate to keep the contacts conducting.

This device structure permits multiple photocurrent spectroscopy modes (see Supporting Information §3). In Auger photocurrent mode, we measure the current I_C that flows from the top electrode through the thin hBN to contact CT1, keeping CT2 disconnected. Similar measurement results were obtained using contact CT2 instead. The I_C−V_T characteristic in the dark (black trace in Figure 1d) is typical for an hBN tunneling barrier of thickness 8 nm with low defect density:[17] the current is negligible at biases smaller than about 4 V and rises rapidly at larger biases due to Fowler−Nordheim tunneling. To have negligible dark current and to avoid degrading the hBN, we keep the magnitude of V_T smaller than 4 V in the following measurements.

Exciton- and Trion-Induced Auger Photocurrent. When a laser of frequency ω is focused to a spot (∼1 μm in diameter) between the contacts, appreciable photocurrent can be generated, depending on V_T and $\hbar\omega$. For example, at $\hbar\omega$ = 1.71 eV (red trace in Figure 1d), photocurrent appears when V_T is more negative than −2 V, rises to a peak at $V_T \approx -2.7$ V,

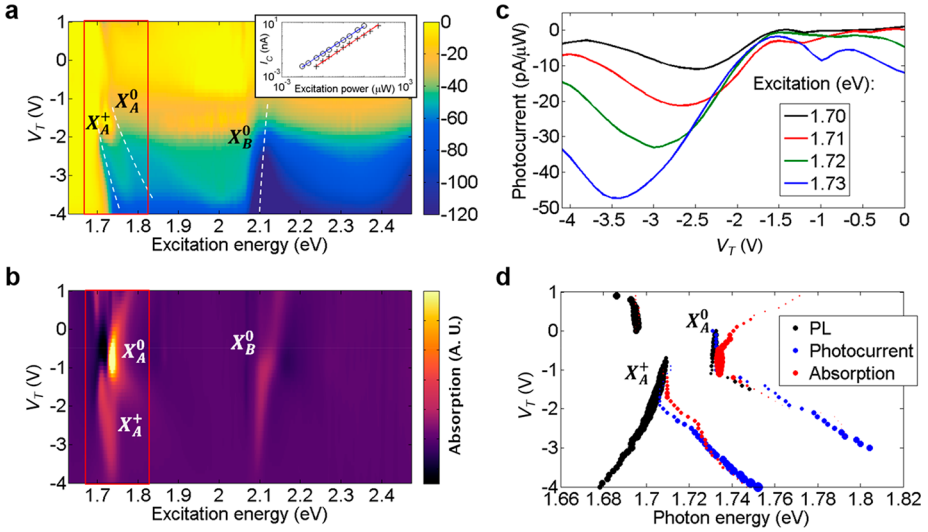

Figure 2. Photocurrent and absorption spectra in the hole-doped regime. (a) Intensity plot of photocurrent I_C as a function of V_T and excitation energy (at V_{BG} = −3 V). White dashed lines indicate positions of the exciton/trion peaks. The A exciton (X_A^0), A trion (X_A^+), and B exciton (X_B^0) features are labeled. Color bar: pA/μW. Inset: peak photocurrent vs excitation power, showing linear behavior, for resonant excitation of X_A^+ (crosses) at 1.725 eV and X_B^0 (circles) at 2.108 eV. (b) Intensity plot of optical absorption strength measured simultaneously with the photocurrent. Color bar: arbitrary linear scale. (c) I_C versus V_T at selected photon energies near the X_A^0 and X_A^+ resonances. (d) Comparison of peak positions extracted from the data in the red boxes in parts a and b and also from photoluminescence measurements (Supporting Information §2).

https://dx.doi.org/10.1021/acs.nanolett.0c02190
Nano Lett. 2020, 20, 5538−5543

and then exhibits negative differential photoconductance[18] (NDPC), decreasing to a minimum at −4 V. The dependence of I_C jointly on V_T and $\hbar\omega$ in the hole-doped regime (V_{BG} = −3 V and V_T ranging negative) is shown as an intensity plot in Figure 2a. A corresponding plot of the optical absorption (see Supporting Information §4) is shown in Figure 2b, where the peaks due to the neutral A and B excitons (X_A^0 and X_B^0) and the positive trion (X_A^+) of monolayer WSe_2 are labeled. Evidently, I_C shows features associated with these absorption resonances (labeled accordingly). In the cases of X_A^0 and X_A^+, I_C exhibits a peak as a function both of $\hbar\omega$ and of V_T. Figure 2c shows traces of I_C versus V_T for selected photon energies close to the trion absorption resonance. Multiple peaks can be seen, each with an associated region of NDPC.

In Figure 2d, we plot the positions of the peaks in both I_C (blue) and absorption (red) for X_A^0 and X_A^+ as a function of $\hbar\omega$ and V_T, derived from the data in the red boxes in Figure 2a and b, respectively. The absorption peaks blue-shift substantially with increasingly negative V_T. This implies a reduction of the exciton/trion binding energy that exceeds the bandgap renormalization, as seen previously.[19] The observation that the X_B^0 peak does not blue-shift with V_T is consistent with this understanding, because the initial electron state for X_B^0 generation is in the lower spin-split valence band far below the Fermi level. The close correspondence between the features in the photocurrent and the absorption strongly implies that the photocurrent is related to the rate of exciton generation. The NDPC occurs when the absorption resonances blue-shift above the excitation energy as V_T increases, thereby reducing the exciton generation rate.

We also plot in Figure 2d, in black, the positions of the X_A^0 and X_A^+ photoluminescence (PL) peaks measured in the same device. At small V_T, they match the absorption peak positions, but as V_T increases, the PL peaks red-shift and so diverge from the blue-shifting absorption peaks. This can be understood as a consequence of the fact that PL is not sensitive to the occupancy of valence band states, combined with free-carrier screening that renormalizes the band gap downward.[20]

Mechanism of Auger Hole Detection. The sign of photocurrent here implies that illumination causes holes to flow from the WSe_2 through the hBN to the top electrode. One possible mechanism for this is direct photoexcitation of holes to states in the WSe_2 valence bands near or below the hBN valence band edge, from which they can simply pass over the barrier. This is energetically possible, since the photon energy is much larger than the WSe_2−hBN valence band offset, $E_{VBO} \sim 0.8$ eV, deduced from recent measurements of WSe_2−graphene[21] and graphene−hBN[22] band offsets. However, direct one-photon absorption is parity forbidden,[23] and moreover, its rate should be independent of excitonic effects. Similar arguments also rule out direct photoactivation of midgap charged defects in hBN. Instead, the fact that the photocurrent has peaks near the exciton absorption resonances implies that it depends on the exciton population, and therefore that the passage of holes through the barrier is assisted by excitons.

In the simplest case, a hole is excited to below the hBN valence band edge by the Auger recombination of a single exciton. This process is energetically possible, since the exciton energy is much greater than E_{VBO}, and unlike for one-photon absorption, the process is not parity forbidden and the rate should be proportional to the exciton population, which is greatest near the absorption resonances. The hole is injected far from the Fermi energy in the graphite, where, as in any metallic electrode, the quasi-particle lifetime is very short and in-plane momentum is not a good quantum number; hence, momentum conservation places no constraint. Since I_C is simply proportional to the laser power (see Figure 2a, inset), this must be the dominant process, because Auger processes involving more than one exciton would produce a superlinear power dependence. With this understanding, using rate equations (see Supporting Information §7), we can estimate a lower bound for the exciton-hole Auger rate of 10^{10} s^{-1}. This is surprisingly large compared with Auger rates in highly doped bulk semiconductors[24] of between 10^6 and 10^8 s^{-1}.

Figure 3a and b show measurements corresponding to those in Figure 2a and b, respectively, but here in the electron-doped

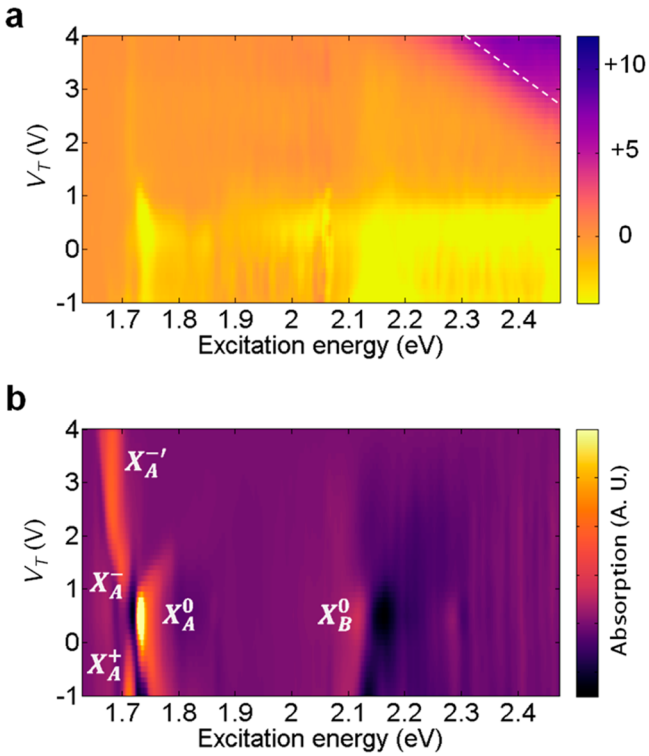

Figure 3. Photocurrent and absorption spectra in the electron-doped regime. (a) Intensity plot of photocurrent I_C as a function of V_T and excitation energy (at V_{BG} = +3 V). Photocurrent is seen only above a threshold indicated by the white dashed line. Color bar: pA/μW. (b) Intensity plot of concurrently measured absorption, with excitonic species labeled.

regime (V_{BG} = +3 V and V_T ranging positive). Unlike in the hole-doped regime, no photocurrent at all is seen for $\hbar\omega < 2.2$ eV, even though a negative trion (X_A^-) resonance is visible at $\hbar\omega \approx 1.7$ eV in the absorption. This is explained by the WSe_2−hBN conduction band offset, E_{CBO}, being much larger than the energy a conduction-band electron can gain by either one-photon absorption or Auger recombination of X_A^-. Using E_{VBOE} = 0.8 eV together with WSe_2 and hBN band gaps of 2.1[25] and 6.0 eV,[26] respectively, gives $E_{CBO} \sim 3.0$ eV. Photocurrent does however flow at higher $\hbar\omega$, above a bias threshold which is indicated by the white dashed line in Figure 3a. This can be explained by direct one-photon absorption by electrons at the WSe_2 conduction band edge,[23] which is parity-allowed, immediately followed by tunneling though the hBN barrier, whose transparency increases with increasing electric field. The

https://dx.doi.org/10.1021/acs.nanolett.0c02190
Nano Lett. 2020, 20, 5538−5543

linear decrease of the bias threshold with $\hbar\omega$ can be reproduced well using the WKB approximation assuming a step height of 3.0 eV that matches E_{CBO} (see Supporting Information §9).

DISCUSSION

The interpretation of the data discussed above is summarized in Figure 4. A schematic of I_C versus V_T traces is plotted in Figure 4a, showing NDPC in the hole-doped regime and photoassisted tunneling in the electron-doped regime. First, consider negative V_T, where the WSe_2 is hole-doped (Figure 4b). When $\hbar\omega$ is resonant with X_A^+, trions are generated (left), and when an electron and a hole in a trion recombine, the excess energy is transferred by an Auger process to the remaining hole, which then has enough energy to pass through the hBN valence band and produce photocurrent (right). Similarly, when $\hbar\omega$ is resonant with X_A^0 or X_B^0, one of the generated neutral excitons can excite a free hole when it recombines,[24] or it can capture a free hole to form a trion and then recombine exciting the hole. Second, consider increasingly negative V_T starting from one of these resonant conditions (Figure 4c). This causes the absorption resonance to blue-shift above $\hbar\omega$, suppressing exciton generation and so reducing the photocurrent, resulting in NDPC. Third, consider positive V_T, where the WSe_2 is electron-doped (Figure 4d). Because of the large E_{CBO}, neither one-photon absorption nor Auger processes can excite electrons to high enough energy to pass into the hBN conduction band. However, at large enough V_T and $\hbar\omega$ (Figure 4d), the barrier transparency for photoexcited electrons is sufficient for photoassisted tunneling to occur and give photocurrent, though without NDPC.

In conclusion, we observe excitation-frequency-dependent photoconductance peaks that result from Auger processes linked to the excitonic absorption resonances in the monolayer semiconductor WSe_2. We find that the dominant Auger process in our WSe_2 heterostructures is excitation of holes by recombination of individual X_A^0 excitons or X_A^+ trions, and we infer a lower bound of 10^{10} s^{-1} on the rate. While the mechanism of hot Auger carrier extraction resembles that considered in other systems,[27−29] our method of using van der Waals heterostructures enables the study of Auger processes at low excitation density and with gate control of the doping.[30] This opens up a window into studying the relatively inaccessible yet vitally important Auger processes. Finally, we note that similar device geometries with hBN-separated FLG gates are used widely for electrostatic gating of 2D semiconductors under optical excitation, and Auger-assisted gate photocurrent should be incorporated as an important factor in analyzing the performance of these devices.

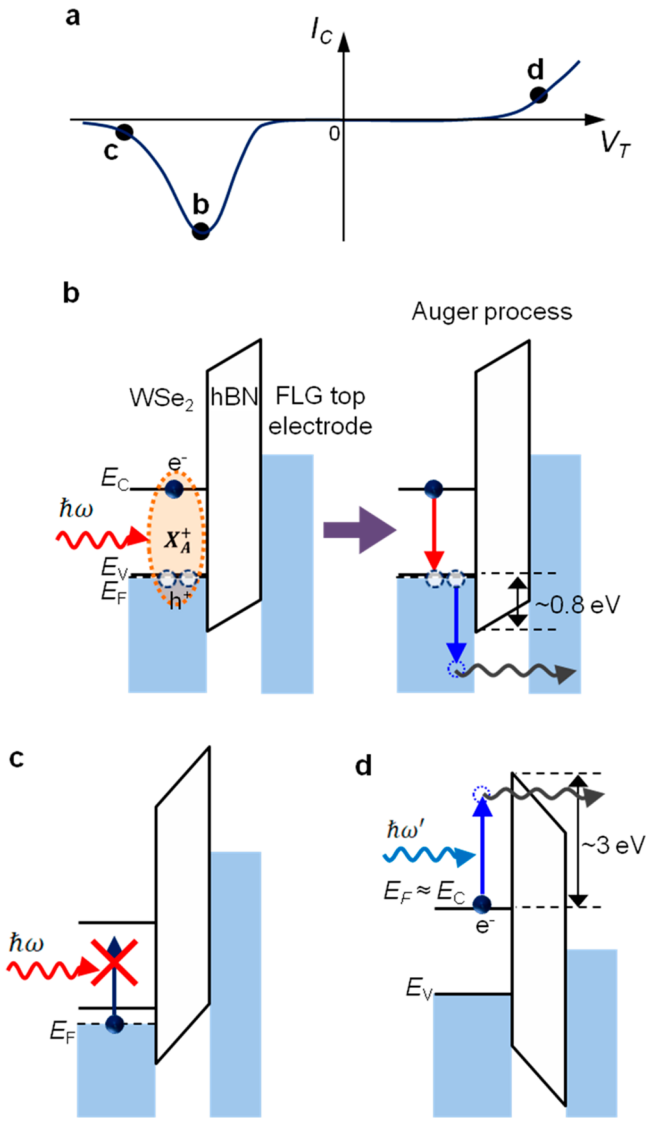

Figure 4. Schematic summary of the NDPC mechanism in the hole-doped regime ($V_T < 0$ V) and photoassisted tunneling in the electron-doped regime ($V_T > 0$ V). (a) A schematic I_C versus V_T trace showing NDPC in the hole-doped regime and photoassisted tunneling in the electron-doped regime. (b) When V_T is negative, the WSe_2 is p-doped. At a certain value of V_T (point b in I_C versus V_T plot), ω is in the middle of the X_A^- absorption resonance and X_A^+ trions are most rapidly created (left panel). Recombination of an electron and hole in a trion causes Auger scattering of the remaining hole to an energy below the hBN valence band edge, allowing it to pass through the hBN producing photocurrent (right panel). (c) As V_T is made more negative (point c), the X_A^+ resonance blue-shifts, causing the rate of creation of excitons and hence the photocurrent to decrease. (d) When V_T is positive, the WSe_2 is n-doped. The large conduction band offset here prevents photoexcitation directly over the barrier, but at large enough V_T (point d), photoexcited electrons can tunnel across the hBN barrier.

METHODS

Device Fabrication. A detailed description of the fabrication process can be found in Supporting Information §1 and §2. In brief, this was accomplished in three stages. In the first, individual flakes were obtained by mechanical exfoliation and identified under an optical microscope. Second, van der Waals assembly was undertaken with the aid of polycarbonate films stretched over viscoelastic stamps. For each device, a total of eight or nine nanoflakes were stacked according to the device geometry shown in Supporting Information §1. Finally, metal electrodes consisting of 10/50 nm vanadium/gold were defined by electron beam lithography and electron beam physical vapor deposition (EBPVD).

Photoluminescence, Photocurrent Spectroscopy, and Charge Modulation Spectroscopy. All measurements presented in the main text were performed in a coldfinger cryostat at a temperature of 5 K. For photoluminescence, a 660 nm beam from a pulsed supercontinuum laser was used, with the average power kept at 10 μW. V_T was varied from −4 to +4

https://dx.doi.org/10.1021/acs.nanolett.0c02190
Nano Lett. 2020, 20, 5538−5543

V; both CT1 and CT2 were grounded, while BG1 and BG2 were disconnected. The emission was collected in reflection geometry and spectrally resolved with a CCD-mounted spectrometer. Photocurrent and charge modulation absorption spectroscopy were performed concurrently with the setup shown in Supporting Information §4. In brief, an ac modulation voltage was added to V_T and the probe laser wavelength was scanned from 500 to 760 nm. The dc component of I_C is measured with a current preamplifier, and the ac component of the probe laser was detected with a Si photodiode connected to a lock-in amplifier. Both supercontinuum and tunable cw sources were used in photocurrent and optical absorption measurements, but no difference was observed in the results. Detailed postprocessing steps and analysis of the optical absorption spectra are given in Supporting Information §5.

■ ASSOCIATED CONTENT

Supporting Information

The Supporting Information is available free of charge at https://pubs.acs.org/doi/10.1021/acs.nanolett.0c02190.

Fabrication steps; device characterization; operating conditions for conventional photocurrent spectroscopy; experimental setup for concurrent Auger photocurrent and charge modulation spectroscopy; CM spectroscopy data postprocessing steps; data from a second device; estimation of exciton-hole Auger recombination rate; and onset of positive photocurrent based on photo-assisted tunneling (PDF)

■ AUTHOR INFORMATION

Corresponding Authors

David Henry Cobden − *Department of Physics, University of Washington, Seattle, Washington 98195, United States;* Email: cobden@uw.edu

Xiaodong Xu − *Department of Physics and Department of Materials Science and Engineering, University of Washington, Seattle, Washington 98195, United States;* orcid.org/0000-0003-0348-2095; Email: xuxd@uw.edu

Authors

Colin Ming Earn Chow − *Department of Physics, University of Washington, Seattle, Washington 98195, United States;* orcid.org/0000-0002-9551-8237

Hongyi Yu − *Guangdong Provincial Key Laboratory of Quantum Metrology and Sensing & School of Physics and Astronomy, Sun Yat-Sen University (Zhuhai Campus), Zhuhai 519082, China; Department of Physics and Centre of Theoretical and Computational Physics, University of Hong Kong, Hong Kong, China*

John R. Schaibley − *Department of Physics, University of Washington, Seattle, Washington 98195, United States; Department of Physics, University of Arizona, Tucson, Arizona 85721, United States*

Pasqual Rivera − *Department of Physics, University of Washington, Seattle, Washington 98195, United States;* orcid.org/0000-0002-5909-1686

Joseph Finney − *Department of Physics, University of Washington, Seattle, Washington 98195, United States*

Jiaqiang Yan − *Materials Science and Technology Division, Oak Ridge National Laboratory, Oak Ridge, Tennessee 37831, United States;* orcid.org/0000-0001-6625-4706

David Mandrus − *Materials Science and Technology Division, Oak Ridge National Laboratory, Oak Ridge, Tennessee 37831, United States; Department of Materials Science and Engineering, University of Tennessee, Knoxville, Tennessee 37996, United States*

Takashi Taniguchi − *National Institute for Materials Science, Tsukuba, Ibaraki 305-0044, Japan;* orcid.org/0000-0002-1467-3105

Kenji Watanabe − *National Institute for Materials Science, Tsukuba, Ibaraki 305-0044, Japan;* orcid.org/0000-0003-3701-8119

Wang Yao − *Department of Physics and Centre of Theoretical and Computational Physics, University of Hong Kong, Hong Kong, China*

Complete contact information is available at: https://pubs.acs.org/10.1021/acs.nanolett.0c02190

Author Contributions

X.X., D.H.C., J.R.S., and C.M.E.C. conceived the experiments. C.M.E.C. fabricated the devices (with the assistance from P.R.), performed the experiments, and analyzed the data, supervised by X.X. and D.H.C. W.Y. and H.Y. proposed the hole-Auger scattering mechanism. J.R.S. conducted preliminary studies on a different sample, fabricated by J.F. J.Y. and D.M. characterized and provided WSe_2 crystals. T.T. and K.W. provided hBN crystals. C.M.E.C., X.X., D.H.C., and W.Y. wrote the manuscript. All authors discussed the results.

Notes

The authors declare no competing financial interest.

The data that support the findings of this study are available from the corresponding author upon reasonable request.

■ ACKNOWLEDGMENTS

This work was mainly supported by AFOSR FA9550-18-1-0104 and FA9550-18-1-0046 and partially supported by NSF EFRI (Grant No. 1741656). The initial measurement was supported by DoE BES (DE-SC0018171) through J.R.S. W.Y. and H.Y. were supported by the Croucher Foundation (Croucher Innovation Award), the RGC of Hong Kong (HKU17305914P), and the HKU ORA. D.M. and J.Y. were supported by DoE BES, Materials Sciences and Engineering Division. K.W. and T.T. acknowledge support from the Elemental Strategy Initiative conducted by the MEXT, Japan, and the CREST (JPMJCR15F3), JST. X.X. acknowledges support from the State of Washington through Clean Energy Institute and from the Boeing Distinguished Professorship in Physics.

■ REFERENCES

(1) Splendiani, A. Emerging Photoluminescence in Monolayer MoS_2. *Nano Lett.* **2010**, *10*, 1271−1275.

(2) Mak, K. F.; Lee, C.; Hone, J.; Shan, J.; Heinz, T. F. Atomically Thin MoS_2: A New Direct-Gap Semiconductor. *Phys. Rev. Lett.* **2010**, *105*, 136805.

(3) Shi, H.; et al. Exciton Dynamics in Suspended Monolayer and Few-Layer MoS_2 2D Crystals. *ACS Nano* **2013**, *7*, 1072−1080.

(4) Kozawa, D.; et al. Photocarrier relaxation pathway in two-dimensional semiconducting transition metal dichalcogenides. *Nat. Commun.* **2014**, *5*, 4543.

(5) Beattie, A. R.; Landsberg, P. T.; Frohlich, H. Auger effect in semiconductors. *Proc. R. Soc. London, Ser. A* **1959**, *249*, 16−29.

(6) Konabe, S.; Okada, S. Effect of Coulomb interactions on optical properties of monolayer transition-metal dichalcogenides. *Phys. Rev. B: Condens. Matter Mater. Phys.* **2014**, *90*, 155304.
(7) Mouri, S.; et al. Nonlinear photoluminescence in atomically thin layered WSe_2 arising from diffusion-assisted exciton-exciton annihilation. *Phys. Rev. B: Condens. Matter Mater. Phys.* **2014**, *90*, 155449.
(8) Kumar, N.; et al. Exciton-exciton annihilation in $MoSe_2$ monolayers. *Phys. Rev. B: Condens. Matter Mater. Phys.* **2014**, *89*, 125427.
(9) Sun, D.; et al. Observation of Rapid Exciton-Exciton Annihilation in Monolayer Molybdenum Disulfide. *Nano Lett.* **2014**, *14*, 5625−5629.
(10) Javaux, C.; et al. Thermal activation of non-radiative Auger recombination in charged colloidal nanocrystals. *Nat. Nanotechnol.* **2013**, *8*, 206−212.
(11) Cunningham, P. D.; McCreary, K. M.; Jonker, B. T. Auger Recombination in Chemical Vapor Deposition-Grown Monolayer WS_2. *J. Phys. Chem. Lett.* **2016**, *7*, 5242−5246.
(12) Robert, C. Exciton radiative lifetime in transition metal dichalcogenide monolayers. *Phys. Rev. B: Condens. Matter Mater. Phys.* **2016**, *93*, 205423.
(13) Wang, H.; Zhang, C.; Rana, F. Ultrafast Dynamics of Defect-Assisted Electron-Hole Recombination in Monolayer MoS_2. *Nano Lett.* **2015**, *15*, 339−345.
(14) Cunningham, P. D.; et al. Charge Trapping and Exciton Dynamics in Large-Area CVD Grown MoS_2. *J. Phys. Chem. C* **2016**, *120*, 5819−5826.
(15) Danovich, M.; Zólyomi, V.; Fal'ko, V. I.; Aleiner, I. L. Auger recombination of dark excitons in WS_2 and WSe_2 monolayers. *2D Mater.* **2016**, *3*, 035011.
(16) Malic, E.; et al. Dark excitons in transition metal dichalcogenides. *Phys. Rev. Mater.* **2018**, *2*, 14002.
(17) Chandni, U.; Watanabe, K.; Taniguchi, T.; Eisenstein, J. P. Evidence for Defect-Mediated Tunneling in Hexagonal Boron Nitride-Based Junctions. *Nano Lett.* **2015**, *15*, 7329−7333.
(18) Choi, K. K.; Levine, B. F.; Bethea, C. G.; Walker, J.; Malik, R. J. Negative differential photoconductance in an alternately doped multiple quantum well structure. *Appl. Phys. Lett.* **1988**, *52*, 1979−1981.
(19) Wang, Z.; Zhao, L.; Mak, K. F.; Shan, J. Probing the Spin-Polarized Electronic Band Structure in Monolayer Transition Metal Dichalcogenides by Optical Spectroscopy. *Nano Lett.* **2017**, *17*, 740−746.
(20) Nguyen, P. V.; et al. Visualizing electrostatic gating effects in two-dimensional heterostructures. *Nature* **2019**, *572*, 220−223.
(21) Wilson, N. R.; et al. Determination of band offsets, hybridization, and exciton binding in 2D semiconductor heterostructures. *Sci. Adv.* **2017**, *3*, No. e1601832.
(22) Britnell, L.; et al. Field-Effect Tunneling Transistor Based on Vertical Graphene Heterostructures. *Science* **2012**, *335*, 947−950.
(23) Liu, G.-B.; Xiao, D.; Yao, Y.; Xu, X.; Yao, W. Electronic structures and theoretical modelling of two-dimensional group-VIB transition metal dichalcogenides. *Chem. Soc. Rev.* **2015**, *44*, 2643−2663.
(24) Nakamura, A.; Morigaki, K. Photoconductivity Associated with Auger Recombination of Excitons Bound to Neutral Donors in Te-Doped Gallium Phosphide. *J. Phys. Soc. Jpn.* **1973**, *34*, 672−676.
(25) Zhang, C.; et al. Probing Critical Point Energies of Transition Metal Dichalcogenides: Surprising Indirect Gap of Single Layer WSe_2. *Nano Lett.* **2015**, *15*, 6494−6500.
(26) Cassabois, G.; Valvin, P.; Gil, B. Hexagonal boron nitride is an indirect bandgap semiconductor. *Nat. Photonics* **2016**, *10*, 262−266.
(27) Barrows, C. J.; et al. Electrical Detection of Quantum Dot Hot Electrons Generated via a Mn^{2+}-Enhanced Auger Process. *J. Phys. Chem. Lett.* **2017**, *8*, 126−130.
(28) Tisdale, W. A.; et al. Hot-electron transfer from semiconductor nanocrystals. *Science* **2010**, *328*, 1543−7.
(29) Pandey, A.; Guyot-Sionnest, P. Hot Electron Extraction From Colloidal Quantum Dots. *J. Phys. Chem. Lett.* **2010**, *1*, 45−47.
(30) Binder, J. Upconverted electroluminescence via Auger scattering of interlayer excitons in van der Waals heterostructures. *Nat. Commun.* **2019**, *10*, 2335.

https://dx.doi.org/10.1021/acs.nanolett.0c02190
Nano Lett. 2020, 20, 5538−5543